Conjugated laminar forced convection in ducts with periodic variation of inlet temperature

W. S. Kim and M. N. Özişik
Mechanical and Aerospace Engineering Department, North Carolina State University, Raleigh, NC, USA

Conjugated laminar forced convection with parabolic velocity profile is studied for flow inside both parallel-plate and circular ducts subjected to a periodically varying inlet temperature. The analysis of this class of problems leads to a Sturm–Liouville type complex eigenvalue problem for which no known solution is available. In this work, a new methodology is presented for a direct solution of such complex eigenvalue problems in the complex domain using the shooting method along with the Runge–Kutta method. The methodology is applicable for solving both laminar and turbulent flow problems; here we consider only the laminar flow with a parabolic velocity profile. The results clearly show that the slug-flow assumption overestimates the phase lag and the Nusselt number. Some benchmark results are also presented for the eigenquantities in tabular form.

Keywords: complex eigenvalue; transient duct flow; conjugated laminar forced convection

Introduction

The periodic Graetz problem is of great interest in engineering applications related to the thermal response of heat exchanger equipment subjected to periodic disturbances on inlet temperature. The solution of a heat transfer problem of this type usually leads to a complex eigenvalue problem for which no known solution is available. The principal difficulty in the analysis of such problems is finding the solution for the resulting complex eigenvalue problem in the complex domain. Kardas[1] investigated the heat transfer to flow in parallel-plate channels subjected to an inlet temperature varying with time. He employed a quasisteady model and Laplace transformation. Sparrow and de Farias[2] considered unsteady laminar heat transfer in a parallel-plate channel with conjugation to the walls. They assumed that fluid inlet temperature varies periodically in a sinusoidal manner with an arbitrary frequency. They also assumed slug flow and utilized a trial-and-error procedure to evaluate numerical value of real and complex parts of the eigenvalues from a system of two coupled nonlinear equations. Cotta *et al.*[3] developed an analytical solution to laminar forced convection in parallel-plate ducts and circular tubes with conjugation to the walls, subjected to periodic time variation in the inlet temperature. They assumed a slug flow and transformed the related complex transcendental equation to a system of two coupled transcendental equations, which they solved by using the recently advanced count method (Mikhailov and Özişik[4]). Kakaç and Yener[5] considered a transient-energy equation with inlet temperature varying over time for slug flow and turbulent heat transfer between two parallel plates, without conjugation with the walls. They presented experimental results to predict the lowest eigenvalue for turbulent flow. Kakaç and Yener[6] also presented a formal solution for laminar parabolic flow with inlet temperature varying over time without performing numerical calculations. They asserted that a frequency-response method described by Kakaç and Yener[7] might be used to experimentally determine only the first eigenvalue. Cotta and Özişik[8] studied laminar forced convection with periodic variations of inlet temperature without conjugation with the walls in both parallel-plate ducts and circular tubes. Susec and Sawant[9] solved the unsteady, conjugated problem for a parallel-plate duct with inlet fluid temperature varying periodically in time by using an improved quasisteady approach.

In this work, we present a direct approach for solving laminar forced convection in parallel-plate ducts and circular tubes for parabolic flow with conjugation to the walls, subjected to periodic variation of inlet temperature over time. We solve directly the resulting complex eigenvalue problem, using a shooting method along with the Runge–Kutta method in the complex domain. We believe that this work is the first attempt to solve directly the complex eigenvalue problems encountered in numerous engineering applications.

Formulation of the problem

We consider laminar forced convection in parallel-plate ducts and circular tubes, subjected periodically varying let temperature. We take conjugation to the wall into account by balancing the heat transfer rate at the wall surface to the rate of energy storage in the wall, and it enters the problem as a time-dependent boundary condition. We assume that the physical properties are constant and that viscous dissipation is negligible. Then, the mathematical formulation of the problem is

$$\frac{\partial T(r,z,t)}{\partial t}+u(r)\frac{\partial T(r,z,t)}{\partial z}=\alpha\frac{1}{r^m}\frac{\partial}{\partial r}\left(r^m\frac{\partial T(r,z,t)}{\partial r}\right) \qquad 0<r<b,\ z>0,\ t>0 \quad (1a)$$

where

$$m=\begin{cases}0 & \text{for parallel-plate duct}\\ 1 & \text{for circular tube}\end{cases}$$

with the inlet condition given by

$$T(r,0,t)=T_o+\Delta T_o e^{i\omega t} \qquad (1b)$$

Address reprint requests to Dr. Özişik at the Mechanical and Aerospace Engineering Department, North Carolina State University, Raleigh, NC 27695-7910, USA.

Received 1 November 1989; accepted 9 February 1990

and the boundary conditions are:

$$\left.\frac{\partial T(r,z,t)}{\partial r}\right|_{r=0}=0 \tag{1c}$$

$$-k\left.\frac{\partial T(r,z,t)}{\partial r}\right|_{r=b}=\rho_w c_w l_w \frac{\partial T_w(z,t)}{\partial t} \tag{1d}$$

$$T(b,z,t)=T_w(z,t) \tag{1e}$$

where

$$i=\sqrt{-1} \tag{2}$$

We are seeking the periodic solution, so we do not need the initial condition. The problem, expressed in the dimensionless form, is

$$\frac{\partial\theta(R,Z,\tau)}{\partial\tau}+W(R)\frac{\partial\theta(R,Z,\tau)}{\partial Z}=\frac{1}{R^m}\frac{\partial}{\partial R}\left(R^m\frac{\partial\theta(R,Z,\tau)}{\partial R}\right)$$

$$0<R<1,\ Z>0,\ \tau>0 \tag{3a}$$

$$\theta(R,0,\tau)=e^{i\Omega\tau} \tag{3b}$$

$$\left.\frac{\partial\theta(R,Z,\tau)}{\partial R}\right|_{R=0}=0 \tag{3c}$$

$$a^*\left.\frac{\partial\theta(R,Z,\tau)}{\partial R}\right|_{R=1}+\left.\frac{\partial\theta(R,Z,\tau)}{\partial\tau}\right|_{R=1}=0 \tag{3d}$$

where, $W(R)$ is the dimensionless velocity profile, or

$$W(R)=\begin{cases}\frac{3}{2}(1-R^2) & \text{for parallel-plate channel} \quad (4a)\\ 2(1-R^2) & \text{for circular duct} \quad (4b)\end{cases}$$

and a^* represents the ratio of heat capacity of fluid to that of the wall, or

$$a^*=\frac{\rho c_p b}{\rho_w c_w l_w} \tag{5}$$

We want a solution in the form

$$\theta(R,Z,\tau)=\tilde{\theta}(R,Z)e^{i\Omega(\tau-Z)} \tag{6}$$

which results in the following problem for the function $\tilde{\theta}(R,Z)$:

$$W(R)\frac{\partial\tilde{\theta}(R,Z)}{\partial Z}=\frac{1}{R^m}\frac{\partial}{\partial R}\left\{R^m\frac{\partial\tilde{\theta}(R,Z)}{\partial R}\right\}-i\Omega\{1-W(R)\}\tilde{\theta}(R,Z)$$

$$0<R<1,\ Z>0 \tag{7a}$$

$$\tilde{\theta}(R,0)=1 \tag{7b}$$

$$\left.\frac{\partial\tilde{\theta}(R,Z)}{\partial R}\right|_{R=0}=0 \tag{7c}$$

$$a^*\left.\frac{\partial\tilde{\theta}(R,Z)}{\partial R}\right|_{R=1}+i\Omega\tilde{\theta}(R,Z)|_{R=1}=0 \tag{7d}$$

Notation

$A_b(Z)$, $A_h(Z)$, $A_w(Z)$	Amplitudes for bulk temperature, heat flux, and wall temperature, respectively
a^*	Defined by Equation 5
b^*	Defined by Equation 20b
b	Radius of circular duct or one half the spacing between parallel plates
$c_k^{(0)}$, $c_k^{(1)}$	Real parts of $\lambda_k^{(0)}$ and $\lambda_k^{(1)}$, respectively
c_p, c_w	Specific heat of fluid and wall, respectively
$d_k^{(0)}$, $d_k^{(1)}$	Imaginary parts of $\lambda_k^{(0)}$ and $\lambda_k^{(1)}$, respectively
$\overline{f_k}$	Defined by Equation 11b
$F(\lambda_k)$	Defined by Equation 20
$F(\lambda_k^{(j)})$	Defined by Equation 23, $(=F_k^{(j)})$
$h(z,t)$	Heat transfer coefficient
i	$\sqrt{-1}$
K	Thermal conductivity
k	Integer $(=1,2,3,\ldots)$
l_w	Wall thickness
N_k	Normalization integral defined by Equation 10
$\mathrm{Nu}(Z,\tau)$	Nusselt number
$q_w(Z,\tau)$	Wall heat flux
r	Radial or normal coordinate
R	Dimensionless normal coordinate $(=r/b)$
t	Time
$T(r,z,t)$	Fluid temperature
$T_w(z,t)$	Wall temperature
T_o	Mean value of inlet temperature cycle
ΔT_o	Amplitude of inlet oscillations
$u(r)$	Flow velocity
$\bar{u}$	Mean flow velocity
$W(R)$	Dimensionless flow velocity $(=u(r)/\bar{u})$
z	Axial coordinate
Z	Dimensionless axial coordinate $(=\alpha z/\bar{u}b^2)$

Greek symbols

α	Thermal diffusivity of fluid
$\theta(R,Z,\tau)$	Dimensionless temperature $(=(T-T_o)/\Delta T_o)$
$\tilde{\theta}(R,Z)$	Separated dimensionless temperature distribution
$\theta_b(Z,\tau)$	Dimensionless bulk temperature
$\overline{\tilde{\theta}_k}(Z)$	Defined by Equation 9b
$\theta_w(Z,\tau)$	Dimensionless wall temperature
λ_k	kth eigenvalue of eigenvalue Problem 8 $(\equiv\mu_k^2)$
$\lambda_k^{(j)}$	jth iteration of λ_k
μ_k	Complex eigenvalues of eigenvalue Problem 8
ε	Specified tolerance
ρ, ρ_w	Fluid and wall density, respectively
ω	Frequency of oscillations
Ω	Dimensionless frequency of oscillations $(=\omega b^2/\alpha)$
τ	Dimensionless time $(=\alpha t/b^2)$
$\psi_k(\mu_k,R)$	Eigenfunctions of eigenvalue Problem 8
$\phi_b(Z)$, $\phi_h(Z)$, $\phi_w(Z)$	Phase lags for bulk temperature, heat flux, and wall temperature, respectively

Superscripts

$\tilde{}$	Separation symbol defined by Equation 6
$\bar{}$	Integral transform with respect to the R variable

Method of solution

We can formally solve the problem considered here by the classical separation of variables or the integral transform technique (Mikhailov and Özişik[4]). However, the resulting eigenvalue problem is a complex nonclassical Sturm–Liouville system, for which no known solution is available. To solve this problem, we consider the following eigenvalue problem:

$$\frac{d}{dR}\left\{R^m \frac{d\psi_k(\mu_k, R)}{dR}\right\}+\{\mu_k^2 W(R)-i\Omega[1-W(R)]\}R^m\psi_k(\mu_k, R)=0 \qquad 0<R<1 \quad (8a)$$

$$\frac{d\psi_k(\mu_k, R)}{dR}=0 \qquad R=0 \quad (8b)$$

$$a^*\frac{d\psi_k(\mu_k, R)}{dR}+i\Omega\psi_k(\mu_k, R)=0 \qquad R=1 \quad (8c)$$

We now utilize the eigenfunctions of this system to define the following integral transform pair.

- Inversion:

$$\tilde{\theta}(R, Z)=\sum_{k=1}^{\infty}\frac{1}{N_k}\psi_k(\mu_k, R)\bar{\tilde{\theta}}_k(Z) \quad (9a)$$

- Transform:

$$\bar{\tilde{\theta}}_k(Z)=\int_0^1 R^m W(R)\psi_k(\mu_k, R)\tilde{\theta}(R, Z)\,dR \quad (9b)$$

where the normalization integral is

$$N_k=\int_0^1 R^m W(R)[\psi_k(\mu_k, R)]^2\,dR \quad (10)$$

We now proceed to the solution of Equations 7. We operate on Equation 7a with the operator,

$$\int_0^1 R^m\psi_k(\mu_k, R)\,dR$$

and utilize eigenvalue Problem 8 and the boundary conditions, Equations 7c and 7d to obtain

$$\frac{d\bar{\tilde{\theta}}_k(Z)}{dZ}+\mu_k^2\bar{\tilde{\theta}}_k(Z)=0 \quad (11a)$$

with the transformed inlet condition, Equation 7b given by

$$\bar{\tilde{\theta}}_k(0)=\int_0^1 R^m W(R)\psi_k(\mu_k, R)\,dR\equiv\bar{f}_k \quad (11b)$$

The solution to Problem 11 is

$$\bar{\tilde{\theta}}_k(Z)=\bar{\tilde{\theta}}_k(0)e^{-\mu_k^2 Z}=\bar{f}_k e^{-\mu_k^2 Z} \quad (12)$$

When we substitute Equation 12 into Equation 9a, the solution for $\tilde{\theta}(R, Z)$ becomes

$$\tilde{\theta}(R, Z)=\sum_{k=1}^{\infty}\frac{1}{N_k}\psi_k(\mu_k, R)\bar{f}_k e^{-\mu_k^2 Z} \quad (13)$$

where N_k and $\bar{f}_k$ are given by Equations 10 and 11b, respectively. Noting that the dimensionless temperature $\theta(R, Z, \tau)$ is related to the function $\tilde{\theta}(R, Z)$ by Equation 6, we evaluate the dimensionless wall temperature $\theta_w(Z, \tau)$ from

$$\theta_w(Z, \tau)=\theta(R, Z, \tau)|_{R=1}=\tilde{\theta}(R, Z)|_{R=1}e^{i\Omega(\tau-Z)} \quad (14a)$$

where

$$\tilde{\theta}(R, Z)|_{R=1}=\sum_{k=1}^{\infty}\frac{1}{N_k}\psi_k(\mu_k, 1)\bar{f}_k e^{-\mu_k^2 Z} \quad (14b)$$

We determine the dimensionless wall heat flux q_w from its definition:

$$q_w(Z, \tau)=-\left.\frac{\partial\theta(R, Z, \tau)}{\partial R}\right|_{R=1}=-\left.\frac{\partial\tilde{\theta}(R, Z)}{\partial R}\right|_{R=1}e^{i\Omega(\tau-Z)} \quad (15a)$$

where

$$-\left.\frac{\partial\tilde{\theta}(R, Z)}{\partial R}\right|_{R=1}=-\sum_{k=1}^{\infty}\frac{1}{N_k}\psi_k'(\mu_k, 1)\bar{f}_k e^{-\mu_k^2 Z} \quad (15b)$$

and the prime denotes differentiation with respect to R. We also determine the dimensionless bulk temperature, θ_b, from its definition:

$$\theta_b(Z, \tau)=(m+1)\int_0^1 R^m W(R)\theta(R, Z, \tau)\,dR$$

$$=e^{i\Omega(\tau-Z)}(m+1)\sum_{k=1}^{\infty}\frac{1}{N_k}(\bar{f}_k)^2 e^{-\mu_k^2 Z} \quad (16)$$

Because Equations 14, 15, and 16 define complex quantities, we can conveniently express the final solutions for the wall temperature, wall heat flux, and average temperature in polar coordinates, respectively, as

$$\theta_w(Z, \tau)=A_w(Z)\exp[i(\Omega\tau+\phi_w(Z))] \quad (17a)$$

$$q_w(Z, \tau)=A_h(Z)\exp[i(\Omega\tau+\phi_h(Z))] \quad (17b)$$

$$\theta_b(Z, \tau)=A_b(Z)\exp[i(\Omega\tau+\phi_b(Z))] \quad (17c)$$

where A's and ϕ's are, respectively, amplitudes and phase lags of oscillations with respect to the inlet condition. We can evaluate Equations 17a–17c by considering the real and imaginary parts of Equations 14, 15, and 16.

In practice, the inlet condition may be either $T-T_o=\Delta T_o\sin\omega t$ or $\Delta T_o\cos\omega t$. In either case, we determine the corresponding real physical quantities for wall temperature, wall heat flux, and average temperature by simply taking the imaginary or real part, respectively, of Equations 14, 15, and 16. Then, we determine the local Nusselt number from its definition:

$$\mathrm{Nu}(Z, \tau)=\frac{h(z, t)\cdot b}{K}=\frac{\left.\dfrac{\partial\theta(R, Z, \tau)}{\partial R}\right|_{R=1}}{\theta_w(Z, \tau)-\theta_b(Z, \tau)} \quad (18)$$

Clearly, once the eigenvalues μ_k, eigenfunctions $\psi_k(\mu_k, 1)$, the derivative $\psi_k'(\mu_k, 1)$, and the quantities, $\bar{f}_k$ and N_k are available, we can determine the numerical values of physical quantities of interest from the expressions given previously.

Solution of the eigenvalue problem

Because the eigenvalue Problem 8 is a complex, nonstandard Sturm–Liouville system, we could not readily handle it by the standard approaches used for solving two-point boundary-value problem. Instead, we recast Problem 8 as an initial-value problem (IVP) in the form:

$$\frac{d}{dR}\left\{R^m\frac{d\psi_k(\mu_k, R)}{dR}\right\}+\{\mu_k^2 W(R)R^m-i\Omega(1-W(R))R^m\}\psi_k(\mu_k, R)=0 \qquad 0<R<1 \quad (19a)$$

$$\left.\frac{d\psi_k(\mu_k, R)}{dR}\right|_{R=0}=0 \quad (19b)$$

$$\psi_k(\mu_k, R)|_{R=0}=1 \quad (19c)$$

where we take $\psi_k(\mu_k, 0)=1$ by considering the normalization condition of the eigenfunction as another initial condition, and we designate Equations 19 as IVP ($\lambda_k \equiv \mu_k^2$). Then, we can consider the boundary condition at $R=1$, as an unknown function of $\lambda_k(\equiv\mu_k^2)$, say,

$$F(\lambda_k)\equiv \left.\frac{d\psi_k(\mu_k, R)}{dR}\right|_{R=1} + ib^*\psi_k(\mu_k, 1) \tag{20a}$$

where

$$b^*=\frac{\Omega}{a^*} \tag{20b}$$

We can then write the boundary-value problem of Equations 8a, 8b, and 8c as

$$F(\lambda_k)=0 \tag{21}$$

In the shooting method, Equation 21 is solved with the secant method rather than Newton's method in order to avoid the need to evaluate $F'(\lambda_k)$, which is less clearly computed than $F(\lambda_k)$ in this problem. The second method, unlike Newton's method, requires two initial approximations, but only one new function is evaluated for each step.

We can derive the secant method from Newton's method by approximating the derivative $\{F(\lambda_k^{(j)})\}'$ by the quotient

$$\frac{F_k^{(j)}-F_k^{(j-1)}}{\lambda_k^{(j)}-\lambda_k^{(j-1)}}$$

where $F_k^{(j)}$ denotes $F(\lambda_k^{(j)})$, λ_k represents the kth eigenvalue, and $\lambda_k^{(j)}$ represents the jth iteration of λ_k. Then, the computational procedure is as follows: Compute, from given initial approximations $\lambda_k^{(0)}$ and $\lambda_k^{(1)}$, the sequence $\lambda_k^{(2)}, \lambda_k^{(3)}, \ldots$ from the recursion relation

$$\lambda_k^{(j+1)}=\lambda_k^{(j)}-\left\{\frac{F_k^{(j)}-F_k^{(j-1)}}{\lambda_k^{(j)}-\lambda_k^{(j-1)}}\right\}^{-1} F_k^{(j)} \tag{22}$$

where

$$F_k^{(j)}=\psi_k'(\lambda_k^{(j)}, 1)+ib^*\psi_k(\lambda_k^{(j)}, 1) \tag{23}$$

Note that, to start the computation of any eigenvalue λ_k, we need to make two initial guesses, each containing a real and an imaginary part, i.e., $\lambda_k^{(0)}\equiv(c_k^{(0)}, d_k^{(0)})$ and $\lambda_k^{(1)}\equiv(c_k^{(1)}, d_k^{(1)})$. To choose the real part $c_k^{(0)}$ we use the results for the slug-flow case and set the initial guess as $c_k^{(0)}=k^2$. Then we perturb this quantity by, say, 10% and choose $c_k^{(1)}=1.1\times c_k^{(0)}=1.1\times k^2$. To make the initial guess for the imaginary part, we again utilize the slug-flow results and choose $d_k^{(0)}=0.01$, perturb this quantity by 10%, and set $d_k^{(1)}=1.1\times d_k^{(0)}=1.1\times 0.01$. Our experiments show that the results are not sensitive to the choice of the complex part $d_k^{(0)}$ and $d_k^{(1)}$. For example, we obtain almost the same eigenquantities by using $d_k^{(0)}=0.1$, 1.0, and 10. Having chosen the two initial guesses $\lambda_k^{(0)}$ and $\lambda_k^{(1)}$ as described, we compute (approximately) $F_k^{(0)}$ by solving the initial-value Problem 19, using the fourth-order Runge–Kutta method and compute $F_k^{(1)}$ in the same way. Then, by Equation 22,

$$\lambda_k^{(2)}=\lambda_k^{(1)}-\left\{\frac{F(\lambda_k^{(1)})-F(\lambda_k^{(0)})}{\lambda_k^{(1)}-\lambda_k^{(0)}}\right\}^{-1} F(\lambda_k^{(1)})$$

$$\lambda_k^{(3)}=\lambda_k^{(2)}-\left\{\frac{F(\lambda_k^{(2)})-F(\lambda_k^{(1)})}{\lambda_k^{(2)}-\lambda_k^{(1)}}\right\}^{-1} F(\lambda_k^{(2)}), \text{ etc.}$$

$$\vdots \qquad\qquad \vdots$$

We repeat this procedure until we find the corresponding correct value of λ_k that satisfies $F_k^{(j)}\le\varepsilon$ for each two initial approximations, i.e., $\lambda_k^{(0)}$ and $\lambda_k^{(1)}$, where ε is a specified tolerance. In general, the difference between two consecutive eigenvalue has the same order of magnitude, so we can check whether we missed roots.

To check the validity of our procedure, we perform the computations for the slug-flow case, because we can easily obtain the eigensystem of the slug-flow case by substituting $W(R)=1$ into Equation 8a for both cases, i.e., parallel-plate channel and circular duct. We compared the results with those of Cotta *et al.*,[3] and Sparrow and de Farias.[2] The eigenvalues from our study agreed within 10^{-3}% with those of Cotta *et al.* Our results, in general, deviated from those of Sparrow and de Farias by 3%, except for one case which deviated by 33%.

We now summarize the algorithm used for calculating the eigenquantities of the complex eigenvalue Problem 8.

- *Step 1:* Make two initial guesses for $\lambda_k^{(0)}$ and $\lambda_k^{(1)}$.
- *Step 2:* Compute $\psi_k(\lambda_k^{(0)}, R)$ and $\psi_k'(\lambda_k^{(0)}, R)$ by solving initial-value Problem 19, using the fourth-order Runge–Kutta method; compute $\psi_k(\lambda_k^{(1)}, R)$ and $\psi_k'(\lambda_k^{(1)}, R)$ in the same way.
- *Step 3:* Evaluate

  $$F(\lambda_k^{(0)})=\psi_k'(\lambda_k^{(0)}, 1)+ib^*\psi_k(\lambda_k^{(0)}, 1)$$

  and

  $$F(\lambda_k^{(1)})=\psi_k'(\lambda_k^{(1)}, 1)+ib^*\psi_k(\lambda_k^{(1)}, 1)$$

- *Step 4:* Compute $\lambda_k^{(j+1)}$ by the secant method:

  $$\lambda_k^{(j+1)}=\lambda_k^{(j)}-\left\{\frac{F(\lambda_k^{(j)})-F(\lambda_k^{(j-1)})}{\lambda_k^{(j)}-\lambda_k^{(j-1)}}\right\}^{-1} F(\lambda_k^{(j)})$$

  where $j=1, 2, 3, \ldots$
- *Step 5:* Solve IVP ($\lambda_k^{(j+1)}$) using the fourth-order Runge–Kutta method.
- *Step 6:* Evaluate

  $$F(\lambda_k^{(j+1)})=\psi_k'(\lambda_k^{(j+1)}, 1)+ib^*\psi_k(\lambda_k^{(j+1)}, 1)$$

  If $F_k^{(j+1)}$ is less than the given tolerance, go to step 1 and repeat the procedure. Otherwise, go to step 4, updating the values of $F_k^{(j)}$ and $\lambda_k^{(j)}$, and repeat the procedure until $F_k^{(j+1)}$ is less than the given tolerance.

Numerical integration should have the same accuracy as the initial-value problem solver. We performed integrations in N_k and $\bar{f}_k$ by Simpson's rule, because the global accuracy $O(h^4)$ of Simpson's rule is the same as that of the fourth-order Runge–Kutta method used here, where h is the spatial step size. Note that all calculations are performed in the complex domain.

Results and discussion

The eigenvalues μ_k, eigenfunctions $\psi_k(\mu_k, 1)$ and its derivative $\psi_k'(\mu_k, 1)$ at $R=1$, and the quantities N_k, and $\bar{f}_k$ are functions of b^* and a^*. Following Sparrow and de Farias,[2] the representative values of the parameters b^* selected are greater than 1, namely, $b^*=1$, 2, 5, 10, 20, and 100, and $a^*=0.001$. Space limitations preclude the complete tabulation for all cases considered here. Therefore we give the values only for two cases (i.e., $b^*=2$, 10) for a parallel-plate channel and a circular duct with a parabolic velocity profile in Tables 1 and 2, respectively. These values can be used in Equations 14, 15, and 16 to calculate numerical values of wall temperature, wall heat flux, and bulk temperature, respectively. The results of Cotta *et al.*[3] and Sparrow and de Farias,[2] obtained under the assumption of slug flow, are easily recovered as special cases by setting $W(R)=1$ in the computation procedure.

In Figure 1, we present wall temperature as a function of time for various values of the parameter b^* for a circular duct at the location $Z=0.02$. As shown, the amplitude of the wall temperature decreases monotonically, and the phase lag increases with increasing value of b^*, because the large thermal

Table 1 First 20 eigenquantities [μ_k, $\psi_k(\mu_k, 1)$, $\psi'_k(\mu_k, 1)$, N_k, and $\bar{f}_k$] for a parallel-plate channel for $a^* = 0.001$

$b^* = 2$

k	μ_k		$\psi_k(\mu_k, 1)$		$\psi'_k(\mu_k, 1)$		N_k		$\bar{f}_k$	
1	1.1146E+00	4.4143E-01	3.5538E-01	-5.0925E-01	-1.0185E+00	-7.1076E-01	7.2255E-01	-1.7761E-01	8.5511E-01	-1.2494E-01
2	3.8789E+00	5.9476E-01	-1.1444E+00	6.3457E-01	1.2691E+00	2.2888E+00	6.6537E-01	2.0913E-02	-1.2318E-01	-1.1714E-01
3	6.9404E+00	4.6416E-01	1.4074E+00	-4.3438E-01	-8.6875E-01	-2.8147E+00	6.0983E-01	2.2997E-02	2.5543E-02	5.5275E-02
4	1.0141E+01	3.6801E-01	-1.5092E+00	3.3467E-01	6.6933E-01	3.0184E+00	5.9684E-01	1.3824E-02	-8.6075E-03	-2.8767E-02
5	1.3380E+01	3.0716E-01	1.5769E+00	-2.8084E-01	-5.6167E-01	-3.1537E+00	5.9285E-01	8.9630E-03	3.9405E-03	1.7447E-02
6	1.6632E+01	2.6584E-01	-1.6307E+00	2.4671E-01	4.9342E-01	3.2613E+00	5.9123E-01	6.2919E-03	-2.1591E-03	-1.1725E-02
7	1.9889E+01	2.3588E-01	1.6763E+00	-2.2272E-01	-4.4544E-01	-3.3526E+00	5.9043E-01	4.6834E-03	1.3265E-03	8.4453E-03
8	2.3150E+01	2.1306E-01	-1.7163E+00	2.0468E-01	4.0937E-01	3.4325E+00	5.8999E-01	3.6393E-03	-8.8150E-04	-6.3896E-03
9	2.6413E+01	1.9502E-01	1.7520E+00	-1.9048E-01	-3.8096E-01	-3.5040E+00	5.8972E-01	2.9212E-03	6.2015E-04	5.0143E-03
10	2.9676E+01	1.8035E-01	-1.7844E+00	1.7892E-01	3.5783E-01	3.5688E+00	5.8955E-01	2.4046E-03	-4.5552E-04	-4.0473E-03
11	3.2940E+01	1.6814E-01	1.8141E+00	-1.6926E-01	-3.3852E-01	-3.6282E+00	5.8944E-01	2.0197E-03	3.4609E-04	3.3406E-03
12	3.6204E+01	1.5781E-01	-1.8415E+00	1.6103E-01	3.2207E-01	3.6830E+00	5.8935E-01	1.7243E-03	-2.7018E-04	-2.8077E-03
13	3.9469E+01	1.4892E-01	1.8671E+00	-1.5392E-01	-3.0783E-01	-3.7341E+00	5.8929E-01	1.4923E-03	2.1568E-04	2.3956E-03
14	4.2734E+01	1.4118E-01	-1.8910E+00	1.4768E-01	2.9535E-01	3.7819E+00	5.8925E-01	1.3064E-03	-1.7540E-04	-2.0699E-03
15	4.6000E+01	1.3437E-01	1.9134E+00	-1.4215E-01	-2.8429E-01	-3.8269E+00	5.8922E-01	1.1549E-03	1.4491E-04	1.8078E-03
16	4.9265E+01	1.2833E-01	-1.9347E+00	1.3720E-01	2.7440E-01	3.8693E+00	5.8919E-01	1.0297E-03	-1.2136E-04	-1.5937E-03
17	5.2530E+01	1.2292E-01	1.9548E+00	-1.3274E-01	-2.6548E-01	-3.9096E+00	5.8917E-01	9.2479E-04	1.0283E-04	1.4164E-03
18	5.5796E+01	1.1805E-01	-1.9739E+00	1.2869E-01	2.5739E-01	3.9479E+00	5.8915E-01	8.3598E-04	-8.8039E-05	-1.2678E-03
19	5.9062E+01	1.1363E-01	1.9922E+00	-1.2500E-01	-2.5000E-01	-3.9844E+00	5.8914E-01	7.6006E-04	7.6061E-05	1.1420E-03
20	6.2327E+01	1.0960E-01	-2.0097E+00	1.2161E-01	2.4322E-01	4.0193E+00	5.8913E-01	6.9459E-04	-6.6246E-05	-1.0345E-03

$b^* = 10$

k	μ_k		$\psi_k(\mu_k, 1)$		$\psi'_k(\mu_k, 1)$		N_k		$\bar{f}_k$	
1	1.3601E+00	1.1565E-01	1.7253E-02	-1.4134E-01	-1.4134E+00	-1.7253E-01	6.3442E-01	-4.0859E-02	7.6332E-01	-3.7558E-02
2	4.5828E+00	2.5936E-01	-7.2762E-02	3.7697E-01	3.7697E+00	7.2762E-01	6.0026E-01	-2.2756E-02	-1.8171E-01	-1.4197E-02
3	7.8029E+00	3.6692E-01	1.5679E-01	-5.8558E-01	-5.8558E+00	-1.5679E+00	5.9928E-01	-1.8245E-02	9.7965E-02	1.6603E-02
4	1.1014E+01	4.5586E-01	-2.6998E-01	7.7392E-01	7.7392E+00	2.6998E+00	6.0029E-01	-1.5247E-02	-6.5309E-02	-1.6892E-02
5	1.4218E+01	5.2960E-01	4.1196E-01	-9.3838E-01	-9.3838E+00	-4.1196E+00	6.0151E-01	-1.2508E-02	4.7747E-02	1.6855E-02
6	1.7414E+01	5.8849E-01	-5.7882E-01	1.0718E+00	1.0718E+01	5.7882E+00	6.0247E-01	-9.7036E-03	-3.6513E-02	-1.6644E-02
7	2.0607E+01	6.3223E-01	7.6204E-01	-1.1675E+00	-1.1675E+01	-7.6204E+00	6.0291E-01	-6.8412E-03	2.8517E-02	1.6215E-02
8	2.3799E+01	6.6104E-01	-9.4957E-01	1.2226E+00	1.2226E+01	9.4957E+00	6.0271E-01	-4.1018E-03	-2.2466E-02	-1.5532E-02
9	2.6993E+01	6.7621E-01	1.1290E+00	-1.2397E+00	-1.2397E+01	-1.1290E+01	6.0193E-01	-1.7083E-03	1.7758E-02	1.4616E-02
10	3.0193E+01	6.7999E-01	-1.2910E+00	1.2266E+00	1.2266E+01	1.2910E+01	6.0075E-01	1.8906E-04	-1.4072E-02	-1.3536E-02
11	3.3400E+01	6.7508E-01	1.4308E+00	-1.1926E+00	-1.1926E+01	-1.4308E+01	5.9938E-01	1.5576E-03	1.1196E-02	1.2380E-02
12	3.6613E+01	6.6410E-01	-1.5479E+00	1.1465E+00	1.1465E+01	1.5479E+01	5.9801E-01	2.4574E-03	-8.9629E-03	-1.1227E-02
13	3.9834E+01	6.4926E-01	1.6445E+00	-1.0951E+00	-1.0951E+01	-1.6445E+01	5.9674E-01	2.9908E-03	7.2338E-03	1.0132E-02
14	4.3061E+01	6.3223E-01	-1.7238E+00	1.0429E+00	1.0429E+01	1.7238E+01	5.9563E-01	3.2615E-03	-5.8932E-03	-9.1260E-03
15	4.6294E+01	6.1419E-01	1.7891E+00	-9.9232E-01	-9.9232E+00	-1.7891E+01	5.9467E-01	3.3558E-03	4.8492E-03	8.2215E-03
16	4.9532E+01	5.9592E-01	-1.8434E+00	9.4486E-01	9.4486E+00	1.8434E+01	5.9387E-01	3.3374E-03	-4.0303E-03	-7.4183E-03
17	5.2773E+01	5.7790E-01	1.8890E+00	-9.0103E-01	-9.0103E+00	-1.8890E+01	5.9320E-01	3.2509E-03	3.3826E-03	6.7099E-03
18	5.6018E+01	5.6044E-01	-1.9279E+00	8.6091E-01	8.6091E+00	1.9279E+01	5.9264E-01	3.1257E-03	-2.8656E-03	-6.0873E-03
19	5.9266E+01	5.4369E-01	1.9615E+00	-8.2436E-01	-8.2436E+00	-1.9615E+01	5.9217E-01	2.9810E-03	2.4488E-03	5.5403E-03
20	6.2515E+01	5.2774E-01	-1.9909E+00	7.9109E-01	7.9109E+00	1.9909E+01	5.9178E-01	2.8288E-03	-2.1097E-03	-5.0593E-03

Table 2 First 20 eigenquantities [μ_k, $\psi_k(\mu_k, 1)$, $\psi'_k(\mu_k, 1)$, N_k, and $\bar{f}_k$] for a circular duct for $a^* = 0.001$

$b^* = 2$

k	μ_k	$\psi_k(\mu_k, 1)$	$\psi'_k(\mu_k, 1)$	N_k	$\bar{f}_k$
1	1.6106E+00 6.2198E-01	2.1593E-01 -4.9536E-01	-9.9072E-01 -4.3187E-01	2.2018E-01 -1.3350E-01	3.4346E-01 -1.1616E-01
2	3.9185E+00 6.3096E-01	-4.7718E-01 2.6284E-01	5.2569E-01 9.5437E-01	9.8972E-02 -7.3763E-03	-5.0711E-02 -4.7056E-02
3	6.6040E+00 4.4369E-01	4.0941E-01 -1.1732E-01	-2.3463E-01 -8.1881E-01	5.4400E-02 -9.3784E-04	7.8083E-03 1.7809E-02
4	9.4035E+00 3.4080E-01	-3.5506E-01 7.3275E-02	1.4655E-01 7.1013E-01	3.7739E-02 -3.4859E-04	-2.2314E-03 -7.8804E-03
5	1.2224E+01 2.8065E-01	3.2009E-01 -5.3449E-02	-1.0690E-01 -6.4018E-01	2.8948E-02 -1.7607E-04	9.1073E-04 4.2449E-03
6	1.5051E+01 2.4108E-01	-2.9548E-01 4.2189E-02	8.4377E-02 5.9097E-01	2.3491E-02 -1.0294E-04	-4.5572E-04 -2.5951E-03
7	1.7879E+01 2.1286E-01	2.7693E-01 -3.4907E-02	-6.9814E-02 -5.5387E-01	1.9769E-02 -6.5959E-05	2.5954E-04 1.7268E-03
8	2.0708E+01 1.9158E-01	-2.6226E-01 2.9800E-02	5.9600E-02 5.2452E-01	1.7066E-02 -4.5069E-05	-1.6157E-04 -1.2203E-03
9	2.3538E+01 1.7487E-01	2.5025E-01 -2.6014E-02	-5.2028E-02 -5.0049E-01	1.5014E-02 -3.2305E-05	1.0731E-04 9.0188E-04
10	2.6367E+01 1.6135E-01	-2.4015E-01 2.3091E-02	4.6182E-02 4.8030E-01	1.3403E-02 -2.4031E-05	-7.4872E-05 -6.9000E-04
11	2.9197E+01 1.5016E-01	2.3150E-01 -2.0765E-02	-4.1531E-02 -4.6300E-01	1.2104E-02 -1.8414E-05	5.4300E-05 5.4262E-04
12	3.2026E+01 1.4070E-01	-2.2396E-01 1.8869E-02	3.7739E-02 4.4793E-01	1.1035E-02 -1.4456E-05	-4.0627E-05 -4.3638E-04
13	3.4856E+01 1.3260E-01	2.1732E-01 -1.7293E-02	-3.4587E-02 -4.3463E-01	1.0140E-02 -1.1580E-05	3.1188E-05 3.5753E-04
14	3.7685E+01 1.2556E-01	-2.1139E-01 1.5962E-02	3.1924E-02 4.2278E-01	9.3787E-03 -9.4356E-06	-2.4461E-05 -2.9755E-04
15	4.0514E+01 1.1938E-01	2.0605E-01 -1.4823E-02	-2.9646E-02 -4.1211E-01	8.7240E-03 -7.8019E-06	1.9540E-05 2.5097E-04
16	4.3344E+01 1.1390E-01	-2.0122E-01 1.3836E-02	2.7673E-02 4.0243E-01	8.1547E-03 -6.5333E-06	-1.5855E-05 -2.1414E-04
17	4.6173E+01 1.0901E-01	1.9680E-01 -1.2974E-02	-2.5947E-02 -3.9360E-01	7.6552E-03 -5.5321E-06	1.3042E-05 1.8457E-04
18	4.9002E+01 1.0460E-01	-1.9275E-01 1.2213E-02	2.4426E-02 3.8550E-01	7.2133E-03 -4.7303E-06	-1.0857E-05 -1.6050E-04
19	5.1831E+01 1.0062E-01	1.8901E-01 -1.1537E-02	-2.3074E-02 -3.7801E-01	6.8197E-03 -4.0801E-06	9.1353E-06 1.4068E-04
20	5.4660E+01 9.6987E-02	-1.8554E-01 1.0932E-02	2.1864E-02 3.7108E-01	6.4668E-03 -3.5468E-06	-7.7581E-06 -1.2418E-04

$b^* = 10$

k	μ_k	$\psi_k(\mu_k, 1)$	$\psi'_k(\mu_k, 1)$	N_k	$\bar{f}_k$
1	1.9014E+00 1.4205E-01	5.3520E-03 -1.0201E-01	-1.0201E+00 -5.3520E-02	1.8808E-01 -2.3359E-02	2.7966E-01 -2.7357E-02
2	4.6858E+00 2.5677E-01	-1.7832E-02 1.3740E-01	1.3740E+00 1.7832E-01	7.6015E-02 -6.9245E-03	-6.2913E-02 -1.2416E-03
3	7.4734E+00 3.4907E-01	3.3334E-02 -1.6161E-01	-1.6161E+00 -3.3334E-01	4.7838E-02 -3.6996E-03	2.9306E-02 3.2431E-03
4	1.0254E+01 4.2783E-01	-5.1814E-02 1.7975E-01	1.7975E+00 5.1814E-01	3.5001E-02 -2.3799E-03	-1.7418E-02 -3.4832E-03
5	1.3026E+01 4.9454E-01	7.3076E-02 -1.9252E-01	-1.9252E+00 -7.3076E-01	2.7650E-02 -1.6558E-03	1.1624E-02 3.4305E-03
6	1.5792E+01 5.4855E-01	-9.6309E-02 1.9952E-01	1.9952E+00 9.6309E-01	2.2874E-02 -1.1866E-03	-8.2397E-03 -3.2944E-03
7	1.8553E+01 5.8876E-01	1.1997E-01 -2.0030E-01	-2.0030E+00 -1.1997E+00	1.9503E-02 -8.5297E-04	6.0227E-03 3.1069E-03
8	2.1312E+01 6.1474E-01	-1.4207E-01 1.9510E-01	1.9510E+00 1.4207E+00	1.6983E-02 -6.0715E-04	-4.4651E-03 -2.8731E-03
9	2.4073E+01 6.2737E-01	1.6083E-01 -1.8511E-01	-1.8511E+00 -1.6083E+00	1.5020E-02 -4.2724E-04	3.3322E-03 2.6037E-03
10	2.6840E+01 6.2878E-01	-1.7529E-01 1.7212E-01	1.7212E+00 1.7529E+00	1.3445E-02 -2.9906E-04	-2.4992E-03 -2.3178E-03
11	2.9613E+01 6.2178E-01	1.8539E-01 -1.5790E-01	-1.5790E+00 -1.8539E+00	1.2156E-02 -2.1028E-04	1.8869E-03 2.0359E-03
12	3.2394E+01 6.0911E-01	-1.9170E-01 1.4382E-01	1.4382E+00 1.9170E+00	1.1084E-02 -1.4990E-04	-1.4378E-03 -1.7735E-03
13	3.5181E+01 5.9304E-01	1.9506E-01 -1.3069E-01	-1.3069E+00 -1.9506E+00	1.0182E-02 -1.0905E-04	1.1081E-03 1.5392E-03
14	3.7975E+01 5.7526E-01	-1.9630E-01 1.1886E-01	1.1886E+00 1.9630E+00	9.4142E-03 -8.1220E-05	-8.6486E-04 -1.3354E-03
15	4.0774E+01 5.5687E-01	1.9606E-01 -1.0841E-01	-1.0841E+00 -1.9606E+00	8.7529E-03 -6.1984E-05	6.8393E-04 1.1609E-03
16	4.3578E+01 5.3860E-01	-1.9485E-01 9.9277E-02	9.9277E-01 1.9485E+00	8.1780E-03 -4.8421E-05	-5.4788E-04 -1.0127E-03
17	4.6386E+01 5.2085E-01	1.9303E-01 -9.1312E-02	-9.1312E-01 -1.9303E+00	7.6741E-03 -3.8643E-05	4.4437E-04 8.8730E-04
18	4.9196E+01 5.0386E-01	-1.9082E-01 8.4366E-02	8.4366E-01 1.9082E+00	7.2287E-03 -3.1435E-05	-3.6462E-04 -7.8110E-04
19	5.2009E+01 4.8773E-01	1.8841E-01 -7.8292E-02	-7.8292E-01 -1.8841E+00	6.8322E-03 -2.6005E-05	3.0243E-04 6.9097E-04
20	5.4824E+01 4.7250E-01	-1.8590E-01 7.2961E-02	7.2961E-01 1.8590E+00	6.4771E-03 -2.1830E-05	-2.5335E-04 -6.1419E-04

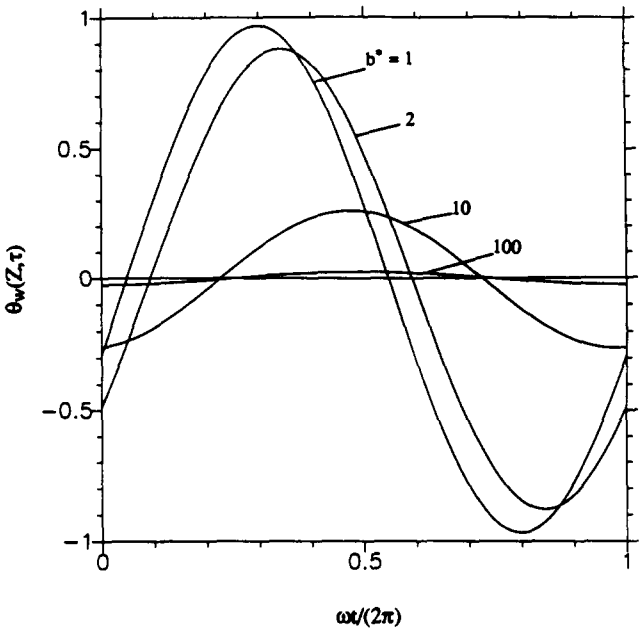

Figure 1 Wall temperature as a function of time at various values of b^* in a circular duct at $Z=0.02$ and $a^*=0.001$

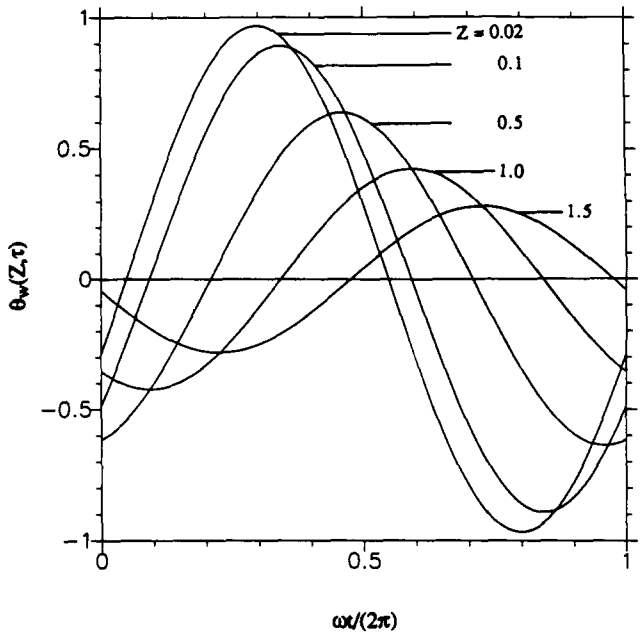

Figure 2 Wall temperature as a function of time at various axial positions for a circular duct at $b^*=1$ and $a^*=0.001$

capacity in the case of large b^* is considered as the large thermal capacity of the wall for a given fluid.

Figure 2 shows wall temperature as a function of time at various axial positions for a circular duct for $b^*=1$. As shown, the amplitude of the timewise variation of wall temperature decreases monotonically, and the phase lag increases with increasing axial distance. These trends are also associated with the wall heat capacity. In Figure 3(a) and (b), we present the amplitude for the wall temperature for a parallel-plate channel and a circular duct, respectively, for $b^*=2$, 5, 10, and 20, with the axial distance along the duct. For comparison, we plotted

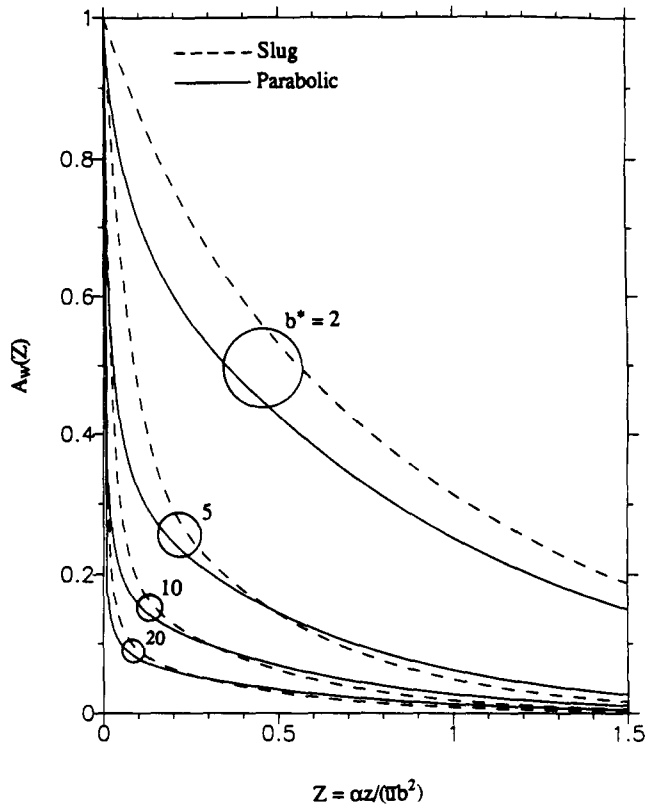

Figure 3(a) Amplitude for wall temperature as a function of axial distance in a parallel-plate channel for various values of b^* and $a^*=0.001$

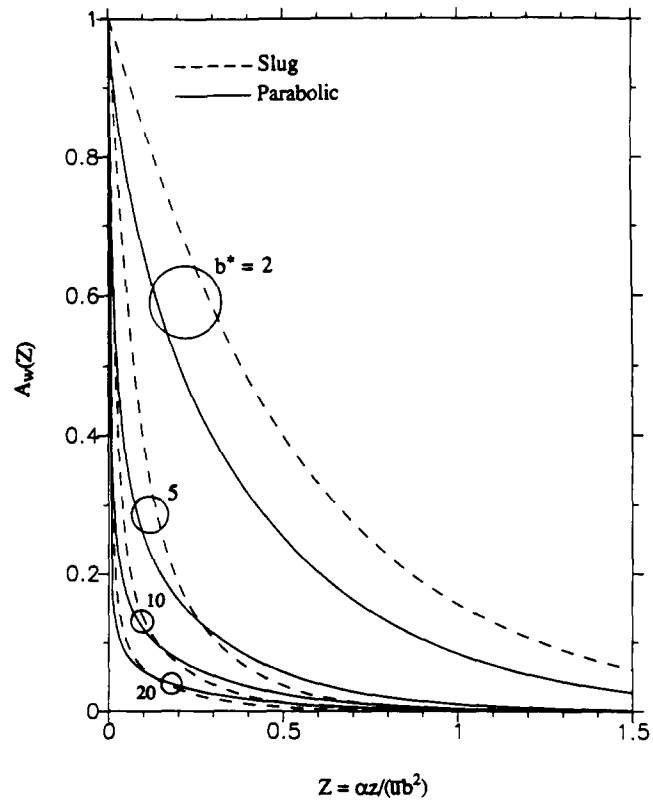

Figure 3(b) Amplitude for wall temperature as a function of axial distance in a circular duct for various values of b^* and $a^*=0.001$

the results for the slug-flow profile. There is a pronounced difference between the results for the slug and parabolic velocity profiles for smaller values of b^*. The parameter b^* can be interpreted as the ratio of rate of energy storage at the wall to heat transfer by conduction across the fluid to or from the wall. For large values of b^* the thermal wave has little penetration along the duct, because it decays rapidly with axial distance. Therefore oscillations in fluid temperature are damped within a short distance from the inlet because of the large thermal capacity of the walls; consequently, the wall temperature oscillation is drastically reduced. For small values of b^*, the thermal wave penetrates farther along the duct, because, being small, the wall thermal capacity requires a longer distance to store the same amount of heat in the wall. Comparison with the results of slug flow clearly shows that the deviation increases with decreasing values of b^*.

Figure 4 shows bulk temperature as a function of time at various axial positions for a circular duct for $b^* = 1$. Note that the amplitude of the timewise variation of bulk temperature decreases monotonically and that the phase lag increases with increasing axial distance, similar to the trends in the wall temperature for $b^* = 1$. Figures 5(a) and (b) and 6(a) and (b) show amplitude for a parallel-plane channel and a circular duct and phase lag for a parallel-plate channel and a circular duct, respectively, for bulk temperature for $b^* = 2$, 5, 10, and 20, with the axial distance along the duct. The results for slug flow are also shown for comparative purposes. Comparison of Figures 5(a) and (b) and 3(a) and (b) shows that attenuation for the wall temperature is much stronger than that for the bulk temperature.

In Figure 7 we present the amplitude variations, with the axial distance along the duct for wall heat flux, for a circular duct and the results for slug flow. For very small axial distances from the inlet, the amplitude of wall heat flux is larger with larger values of b^*, because the temperature gradients are steeper owing to the pronounced attenuation in the wall temperature as shown in Figure 3(a) and (b). At large distances from the inlet, the amplitude of heat flux decreases with increasing b^*.

Figure 8 shows the variations of Nusselt number as a function

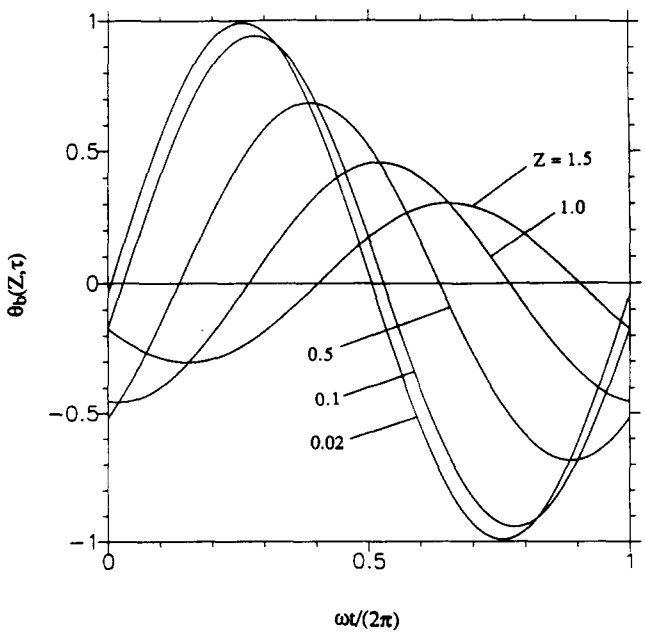

Figure 4 Bulk temperature as a function of time at various axial positions for a circular duct at $b^* = 1$ and $a^* = 0.001$

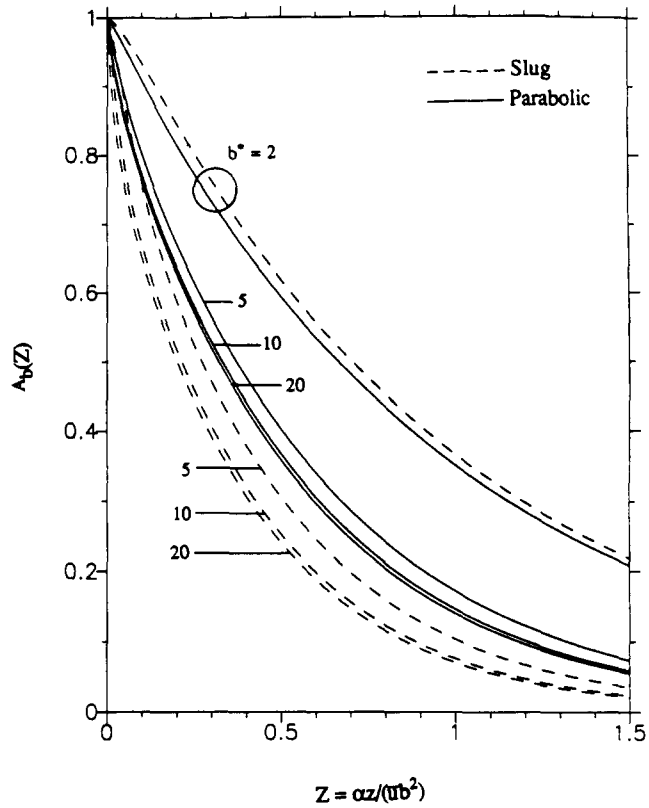

Figure 5(a) Amplitude for bulk temperature as a function of axial distance in a parallel-plate channel for various values of b^* and $a^* = 0.001$

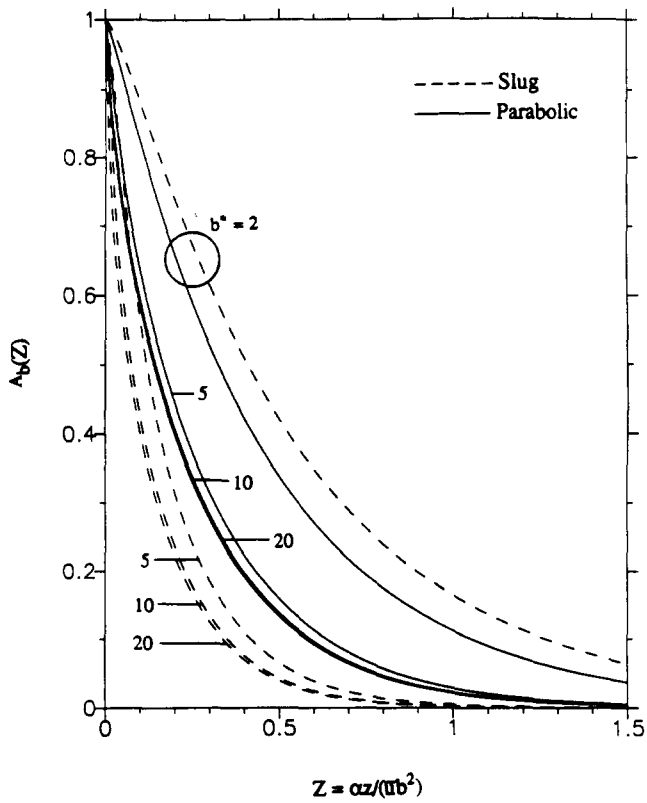

Figure 5(b) Amplitude for bulk temperature as a function of axial distance in a circular duct for various values of b^* and $a^* = 0.001$

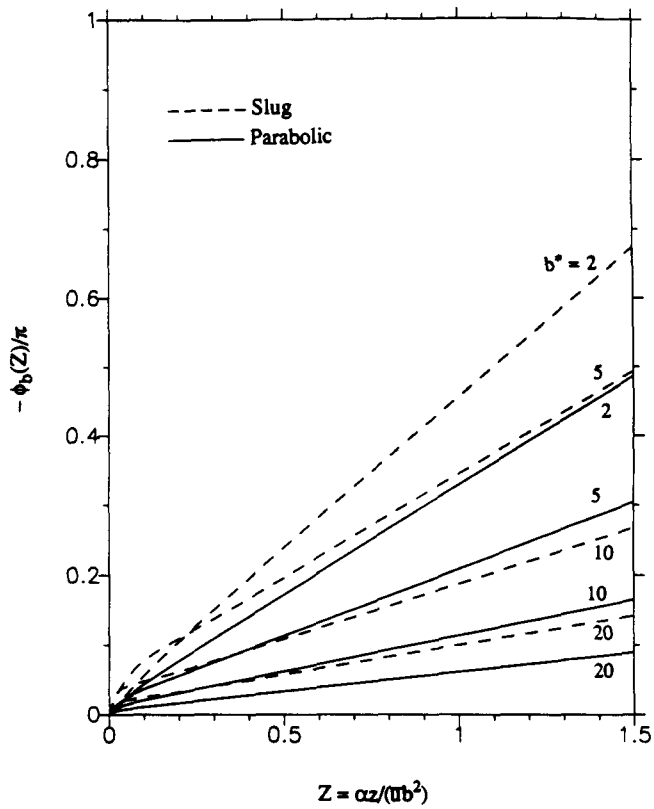

Figure 6(a) Phase lag for bulk temperature as a function of axial distance in a parallel-plate channel for various values of b^* and $a^* = 0.001$

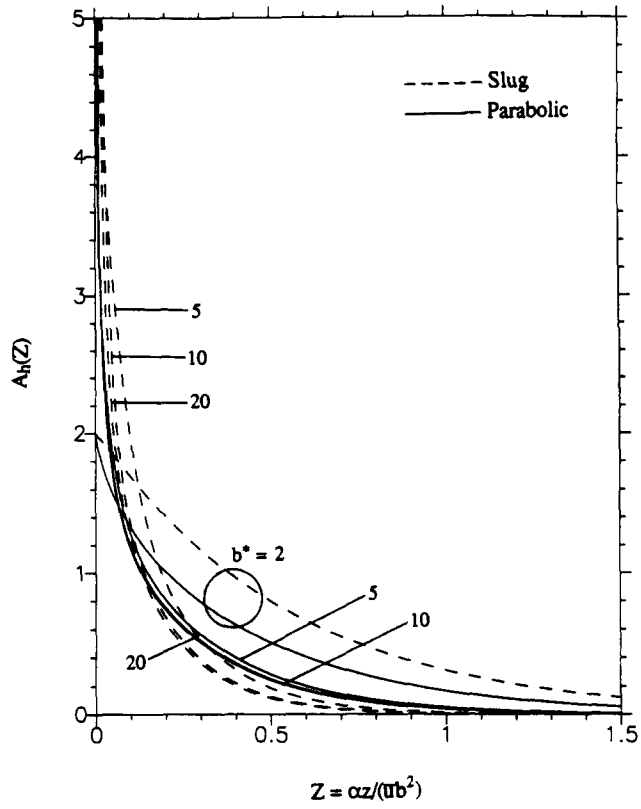

Figure 7 Amplitude for wall heat flux as a function of axial distance in a circular duct for various values of b^* and $a^* = 0.001$

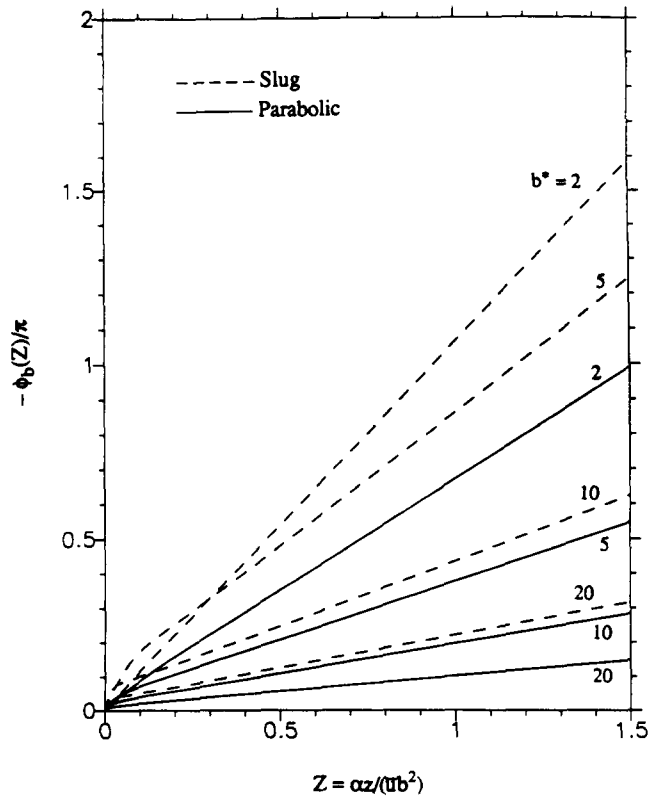

Figure 6(b) Phase lag for bulk temperature as a function of axial distance in a circular duct for various values of b^* and $a^* = 0.001$

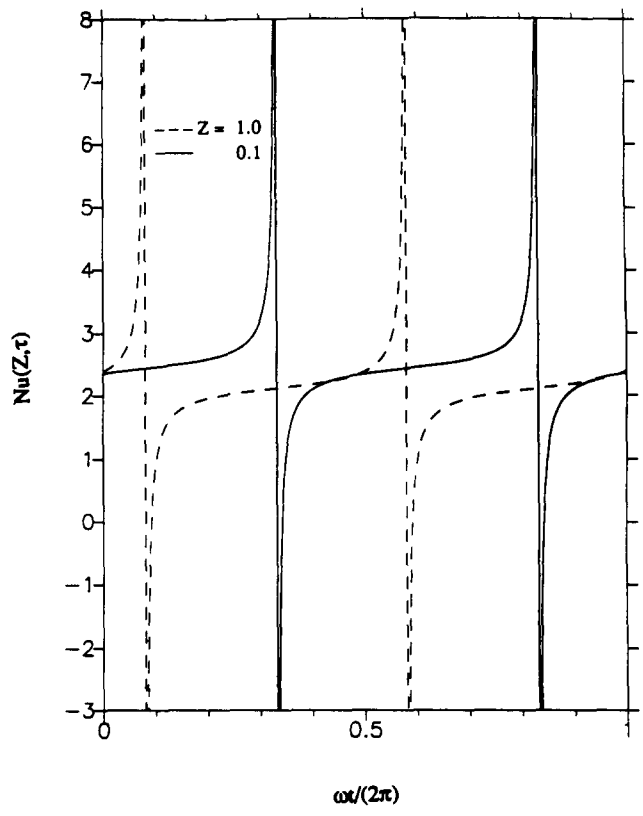

Figure 8 Local Nusselt number as a function of time in a circular duct at $b^* = 1$ and $a^* = 0.001$

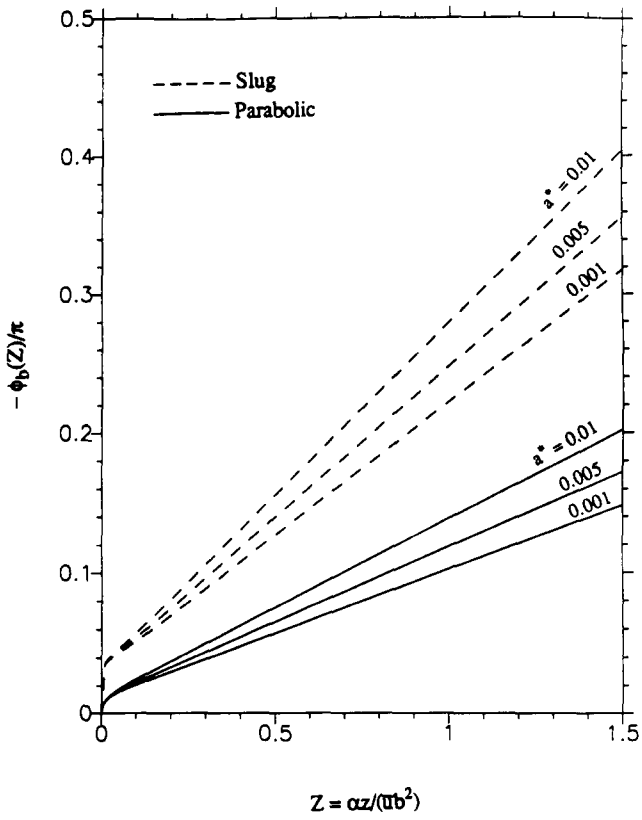

Figure 9 Effects of the parameter a^* on phase lag of the bulk temperature for flow in a circular duct

of time for $Z = 0.1$ and 1.0, at $b^* = 1$ and $a^* = 0.001$, for a circular duct. The sharp discontinuities (i.e., large differences at the discontinuity points) occur when wall and bulk temperatures are close but the heat flow is not zero. The Nusselt number is positive for the heat flux from the wall to the fluid with $\theta_b < \theta_w$. At the instant when θ_b becomes greater than θ_w, the heat flow maintains its direction for a very short time, while $\theta_b > \theta_w$, which implies a negative Nusselt number. Then, the heat flow changes direction, while $\theta_b > \theta_w$, which implies a positive Nusselt number.

We also examined the effects of the parameter a^*, characterizing the ratio of heat capacities of fluid to that of the wall, on the amplitudes and phase lags of bulk temperature, wall temperature, and wall heat flux for both a parallel-plate channel and a circular duct. As pointed out by Sparrow and de Farias,[2] for the flow of a gas in a duct with a metallic wall, the representative values of a^* are much smaller than 1. Therefore, for the flow of a gas in a metallic duct, we chose the values of a^* as 0.001, 0.005, and 0.01. As in the slug-flow case, the variation in a^* has little effect on phase lag for small values of b^*. For the values of a^* considered here, the amplitudes are identical within the scale of Figure 9 for the bulk temperature, wall temperature, and wall heat flux. As a representative case, we present in Figure 9 the effects of a^* on the phase lag of bulk temperature for flow in a circular tube for $b^* = 20$. The results for slug flow show that it overestimates the phase lag. The phase lag increases with increasing axial distance and increasing a^*. We can explain these observations by utilizing the definition of a^*, which represents the ratio of the heat capacity of the fluid to that of the wall. For a given heat capacity of the wall, increasing a^* represents increasing thermal capacity for the fluid, hence relatively large thermal storage in the fluid, which in turn delays the information reaching to both wall and fluid.

Acknowledgment

This work was supported by an Alcoa Foundation Grant of the Alcoa Technical Center, Alcoa Center, PA.

References

1 Kardas, A. On a problem in the theory of the unidirectional regenerator. *Int. J. Heat Mass Transfer*, 1966, **9**, 567–579
2 Sparrow, E. M. and de Farias, F. N. Unsteady heat transfer in ducts with time-varying inlet temperature and participating walls. *Int. J. Heat Mass Transfer*, 1968, **11**, 837–853
3 Cotta, R. M., Mikhailov, M. D., and Özişik, M. N. Transient conjugated forced convection in ducts with periodically varying inlet temperature. *Int. J. Heat Mass Transfer*, 1987, **30**, 2073–2082
4 Mikhailov, M. D. and Özişik, M. N. *Unified Analysis and Solutions of Heat and Mass Diffusion*, Wiley, New York, 1984
5 Kakaç, S. and Yener, Y. Exact solution of the transient forced convection energy equation for timewise variation of inlet temperature. *Int. J. Heat Mass Transfer*, 1973, **16**, 2205–2214
6 Kakaç, S. and Yener, Y. Transient laminar forced convection in ducts. *Low Reynolds Number Flow Heat Exchangers* (S. Kakac, R. K. Shah and A. E. Bergles, Eds.), Hemisphere, New York, 1983, 205–227
7 Kakaç, S. and Yener, Y. Frequency response analysis of transient turbulent forced convection for timewise variation of inlet temperature. *Turbulent Forced Convection in Channels and Bundles* (S. Kakaç and D. B. Spalding, Eds.), Hemisphere, New York, 1979, 865–880
8 Cotta, R. M. and Özişik, M. N. Laminar forced convection inside ducts with periodic variation of inlet temperature. *Int. J. Heat Mass Transfer*, 1986, **29**, 1495–1501
9 Sucec, J. and Sawant, A. M. Unsteady, conjugated, forced convection heat transfer in a parallel plate duct. *Int. J. Heat Mass Transfer*, 1984, **27**, 95–101